ELSEVIER

Effect of Melt Superheat on Maximum Nuclei Density in A356 Alloy

R. Venkataramani, R. Simpson, and C. Ravindran
Center for Near-Net-Shape Processing of Materials, Ryerson Polytechnic University, Toronto M5B 2K3 Canada

The macro-micro modeling, in its present form, does not include the effect of melt superheat. In this work, identical castings of sand, permanent mold, and lost foam processes were produced by pouring aluminum alloy A356 at 700, 750, 800, 850, and 900°C. Grain size increased with pouring temperatures to different levels in the three processes. Cooling rates decreased with increasing pouring temperatures in sand and lost foam castings. Simulated cooling rates agreed closely with experimental values. The grain size-cooling rate relationship agreed well with published data. Maximum nuclei density, n_0, varied with the casting process and pouring temperatures.

INTRODUCTION

Cast iron and aluminum alloys together constitute a major percentage of automotive castings in heavier and lighter sections, respectively. Among the aluminum alloys being used for automotive and aerospace applications, aluminum-silicon alloys are gaining prominence. This is mainly due to their higher strength-to-weight ratios, better castability, better surface finish, and better wear resistance relative to other aluminum alloys. With the increasing trend to produce components of higher strength-to-weight ratios, an increase in the role of aluminum-silicon alloys in automotive castings can be envisaged. A global need for conservation of energy, material, manufacturing costs, and section thickness has resulted in renewed interest in near-net-shape processes enabling such advantages, not usually possible with conventional sand-casting processes.

Prediction of microstructure in a casting helps to estimate mechanical properties of the cast component. Among the models that are available to predict the microstructure in a solidifying casting, some [1, 2] are deterministic while others [3, 4] are probabilistic. Among the deterministic models, the macro-micro modeling approach is gaining impetus for Al-Si alloys [1] and for cast iron [2]. In macro-micro models, the overall energy conservation equations are solved at the macro level for the casting and the mold domain using numerical methods such as finite difference, finite element, and boundary element. At the micro level, equations conserving energy and solute are solved taking the nucleation of solid particles and their subsequent growth during solidification into consideration. This modeling enables prediction of microstructural parameters such as grain size and dendrite arm spacings at different locations in the solidifying casting. Additionally, this allows prediction of temperature profiles with reasonable accuracy.

Superheat is an important parameter for control of cast microstructure. In castings, grain size increases with superheat by reducing the number of nuclei available for growth [5]. The macro-micro model in its present form does not consider the influence

Presented at the International Metallographic Society Symposium on "Microstructural Characterization of Lightweight Materials for Transportation," Montreal, July 24-25, 1994.

MATERIALS CHARACTERIZATION 35:81-92 (1995)

655 Avenue of the Americas, New York, NY 10010
1044-5803/95/$9.50
SSDI 1044-5803(95)00068-A

of superheat on the extent of nucleation. In an earlier article [6], the effect of melt superheat in permanent mold casting was discussed and a methodology to incorporate the same in the macro-micro model was delineated for Al-7%Si alloys.

Many processes are being adopted to produce aluminum-silicon alloy castings. Among them, lost foam casting is popular as a near-net-shape process for automotive and aerospace applications [7]. In the present work, sand, permanent mold, and lost foam casting processes were compared with particular interest in the effect of melt superheat on the maximum nuclei density, n_0 (for definitions of nomenclature, see the Appendix). An equiaxed dendritic growth model was considered in the present analysis.

THEORY

NUCLEATION

Heterogeneous nucleation occurs when the liquid metal crosses the liquidus temperature. The nucleation rate, $\dot{n}$, at a given undercooling, ΔT, can be written in accordance with the heterogeneous nucleation theory [8]:

$$\dot{n} = K_1(N - n) \cdot \exp\left[\frac{-K_2}{T\Delta_{T^2}}\right], \quad (1)$$

where n is the number of nuclei, N is the number of sites available for nucleation, T is the temperature, and K_1 and K_2 are constants. K_1, K_2, and N are constants for a specific type (regarding its wettability), size, and shape of the nucleating site. Stefanescu and Kanetkar [2] have assumed an instantaneous nucleation model based on Eq. (1) to predict the grain size in cast iron. Liquid-aluminum-foundry alloys contain a multitude of foreign particles and substrates ranging from oxides to spinels to the wall of the mold itself [9]. Hence, nucleation can occur practically at any temperature below the liquidus.

Oldfield [10] proposed the theory of continuous nucleation and assumed the following relationship:

$$n = A\Delta T^2, \quad (2)$$

where A is a constant (depending upon type of dendrite: equiaxed or columnar). Goettsch and Dantzig [11] have assumed the number of nuclei per unit volume to be an algebraic function of the nuclei radius. Rappaz [1] and Thévoz [12] have assumed a Gaussian distribution relating $\partial n/\partial\Delta T$ to undercooling, ΔT:

$$\frac{\partial n}{\partial \Delta T} = \frac{n_0}{\sqrt{2\pi}\Delta T_\sigma} \cdot \exp\left[-\frac{(\Delta T - \Delta T_N)^2}{2\Delta T_\sigma^2}\right] \quad (3)$$

where n is the number of nuclei present per unit volume, n_0 is the maximum number of nuclei that can be present per unit volume, ΔT_N is the undercooling corresponding to the peak of the Gaussian distribution, and ΔT_σ is the range of the Gaussian. The number of nuclei present per unit volume and the Gaussian distribution are drawn as functions of ΔT in Fig. 1. Here, $\beta = \sqrt{2\pi}(\Delta T_\sigma/n_0)$.

The three values n_0, ΔT_N, and ΔT_σ together fix the Gaussian curve. These values depend on the alloy system and are influenced by the melt superheats. As the metal or alloy is heated to temperatures higher than the liquidus and then cooled, the cooling rates are affected. The effective number of sites available for nucleation is also affected. Grain size is significantly influenced by superheat [5, 8, 13, 14]. The decrease in the number of nuclei with increasing pouring temperature is attributed to enhanced diffusion of nucleants at higher temperatures, resulting in coalescence of sites [5]. The maximum number of sites available for nucleation, n_0, has been reported to be in the range of 1.02×10^8 to $1.05 \times 10^8 m^{-3}$ [15]. With grain refinement, it has been reported to increase to a range of 10^{11} to $10^{12} m^{-3}$. This shows a strong dependence of n_0 on the melt history.

Merchant [14] has drawn attention to the difficulty in identifying the exact nucleating agent (site). Hence, there is an experimental uncertainty in determining the influence of melt superheats on different types of nucleating agent. In the Gaussian curve shown in Fig. 1, ΔT_N was assumed to remain unaffected by melt superheat. This assumption is justified if melt superheat has identical influence on different types of nucleating sites and if there is no preferential loss of one type or size of nuclei.

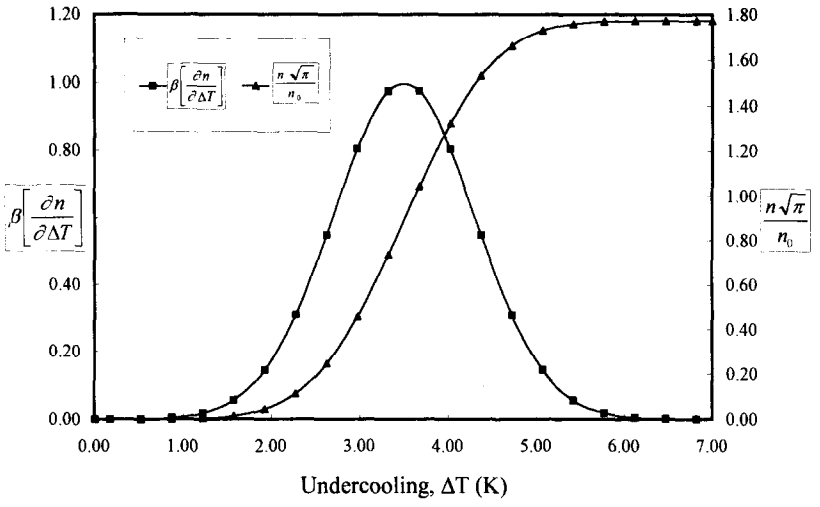

FIG. 1. Variation of Gaussian and error functions with undercooling.

EXPERIMENTAL PROCEDURE

Experiments were conducted on A356 alloy, the composition of which is provided in Table 1. A weighed quantity of the alloy was heated to 50°C higher than the pouring temperature and held for 10 minutes. Since the holding temperature and time also affect the nucleating sites [16], this procedure was repeated in all the cases. Degassing was avoided to obviate any deleterious effect on nucleating sites. The metal was poured at the required temperature into the mold cavity.

Similar castings (20mm diameter × 95mm height) were produced through sand (Fig. 2), permanent mold (Fig. 3), and lost foam (Fig. 4) processes. To avoid its influence on nucleation, refractory coating was not applied on permanent molds. The foam pattern chosen for this set of experiments is shown in Fig. 4. The foam material was expandable polystyrene of 20.6kg m^{-3} (1.6lb ft^{-3}) density. The foam pattern was cut with a hot wire followed by dipping in a refractory slurry of controlled specific gravity (70Bé). The coating thickness was 0.3mm. It was dried in an oven held at 54°C for 8 h. Air was recirculated in the oven. The pattern was placed in the casting flask. The flask was filled with silica sand of 35 American Foundrymen's Society-Grain Fineness Number (AFS-GFN). To compact the sand around the pattern, the flask was subjected to a horizontal vibration at 2 *g* for 5 minutes.

Three chromel-alumel thermocouples were inserted into each casting as shown in Figs. 2–4. The thermocouples were attached to a data acquisition system. The data acquisition system was set to a resolution of 0.1°C. The temperatures were recorded dynamically and the extents of maximum undercooling, ΔT_{max}, measured. The metal was poured at 700, 750, 800, 850, and 900°C. Three trials were carried out for each pouring temperature and casting process and, therefore, each point on the experimental curve is an average of three values.

GRAIN SIZE MEASUREMENTS

The castings were sliced close to the thermocouples, polished, and etched with Tucker's reagent [17]. The grain size was determined

Table 1 Chemical Composition of A356 Aluminum Alloy (wt.%)

Si	*Zn*	*Ti*	*Ni*	*Fe*	*Cu*	*Mg*	*Mn*	*Cr*	*Pb, Be*	*Al*
7.04	0.1	0.14	0.03	0.5	0.14	0.42	0.16	0.05	Traces	Rest

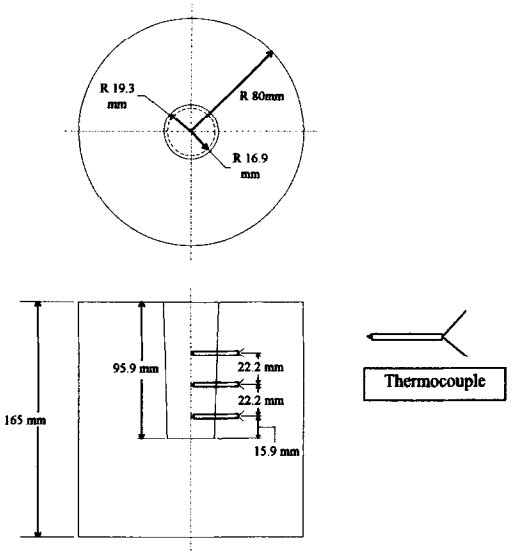

FIG. 2. Sand casting.

using a macroscope by the linear intercept method. The sample was illuminated from several positions to minimize possible errors.

DETERMINATION OF ΔT_{max}

The macrostructure is related to ΔT_{max} at any location within the solidifying casting. This maximum undercooling is the differ-

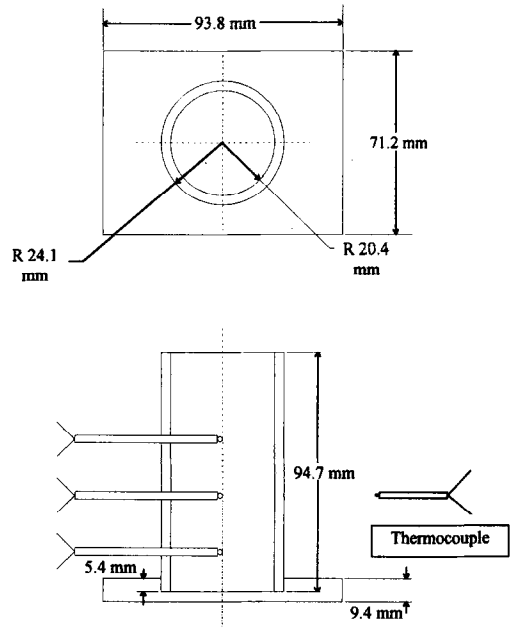

FIG. 3. Permanent mold casting.

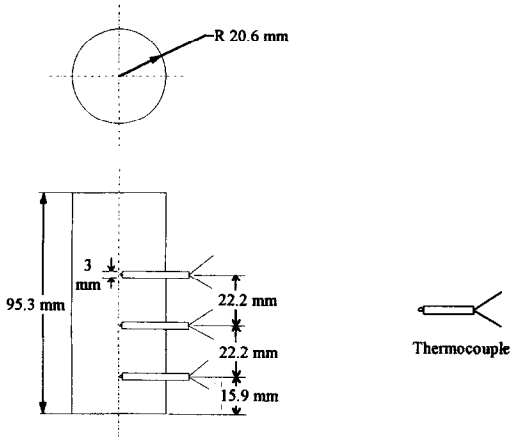

FIG. 4. Lost foam casting.

ence between the theoretical liquidus temperature T_L and the temperature of onset of recalescence T_1. Su and Tsai [18] have highlighted a method to determine the liquidus and solidus temperatures from the cooling curves. This method was adopted in the present work. According to this method, the natural logarithm of the nondimensional temperature was calculated from the cooling curves and plotted with time. The nondimensional temperature, Y, is defined as

$$Y = \frac{T - T_\infty}{T_i - T_\infty}, \tag{4}$$

where T_i is the initial temperature, T_∞ is the ambient temperature, and T is the temperature under consideration. The slope of this curve, that is, $\partial(\ln Y)/\partial t$, was also plotted with time. The liquidus temperature was taken as that temperature at which a kink in this curve was observed just above the onset of recalescence. This method was adopted to determine the liquidus temperature, T_L. The temperature of the onset of recalescence, T_1, was determined as that temperature at which the slope of the cooling curve became zero. ΔT_{max} was then calculated as the difference between T_L and T_1:

$$\Delta T_{max} = T_L - T_1. \tag{5}$$

DETERMINATION OF n_0

The n_0 values were calculated using ΔT_{max} and the actual grain radius observed, R_a, at

that location. The number of nuclei that would be present per unit volume, n_a, is defined as

$$n_a = \frac{1}{\frac{4}{3}\pi R_a^3}. \quad (6)$$

From Eq. (3), the relationship between n_a and ΔT_{max} can be found as:

$$n_a = \frac{n_0}{\sqrt{2\pi}\Delta T_\sigma} \cdot \int_0^{\Delta T_{max}} \exp\left[-\frac{(\Delta T' - \Delta T_N)^2}{2\Delta T_\sigma^2}\right] \cdot d\Delta T', \quad (7)$$

where $\Delta T'$ is the instantaneous undercooling.

If the values ΔT_N and ΔT_σ are assumed to remain unaffected by melt superheat, the relationship between n_0, n_a, and ΔT_{max} can be written as

$$\frac{n_0}{\sqrt{\pi}} = \frac{n_a}{\text{erf}(\xi)}, \quad (8)$$

where

$$\xi = \left[\frac{(\Delta T_{max} - \Delta T_N)}{\sqrt{2}\Delta T_\sigma}\right]. \quad (9)$$

Since ξ can be calculated and n_a is known, the value of n_0 can be determined.

RESULTS AND DISCUSSION

GRAIN SIZE

In general, the grain size is affected by ΔT_{max}. However, ΔT_{max} is affected both by the cooling rate at the liquidus temperature and by the number of sites available for nucleation. The relationship between the grain size, n_0, and ΔT_{max} is given by Eq. (7). When metal is poured at different temperatures, cooling rates as well as the number of nucleation sites are affected. It is well known that for a constant cooling rate, as n_0 decreases, ΔT_{max} increases, leading to an increase in the grain size [12]. Similarly, for a constant n_0, as cooling rate increases, ΔT_{max} increases, leading to a decrease in grain size [19], which can also be seen from Eq. (1).

The metal has to be poured at different temperatures to study the effects of melt superheat. Pouring the metal at different temperatures leads to two aspects: (a) changing the number of nucleation sites of the melt and (b) changing the cooling rate at the liquidus temperature in the solidifying casting. The effect of one cannot be separated from the other.

The macrostructure of the specimens corresponding to the three processes is shown for a typical pouring temperature of 800°C in Fig. 5. Grain sizes of the lost foam and the sand castings are larger than that of the permanent mold casting.

The variations of grain size with pouring temperatures are shown in Fig. 6. Grain size increases with pouring temperatures in all three casting processes though the extent of the variation differs from one process to another. The lost foam cast grain size corresponding to a pouring temperature of 700°C is lower than that of the corresponding sand cast while the grain size becomes progressively coarser with higher pouring temperatures. In the lost foam casting process, the metal loses a certain amount of superheat in degrading the foam pattern. The enthalpy of degradation for expanded polystyrene is $2.9 \times 10^7 \text{Jm}^{-3}$, which leads to a temperature drop of 11°C in the metal [20]. This temperature drop gains significance at lower pouring temperatures (lower superheats). At higher pouring temperatures, however, the drop of 11°C does not alter the grain size considerably. The decreased rate of heat transfer across the refractory coating leads to a coarser grain size in lost foam casting compared to that of sand casting at higher pouring temperatures. The grain size of the permanent mold casting when poured at 900°C is considerably larger than those at lower pouring temperatures. This can be attributed to the inability of the mold to extract additional heat at higher temperatures.

COOLING RATES

Cooling rates were calculated from the experimental data to study the effects of pouring temperature. The rates were obtained close to the liquidus temperature (between

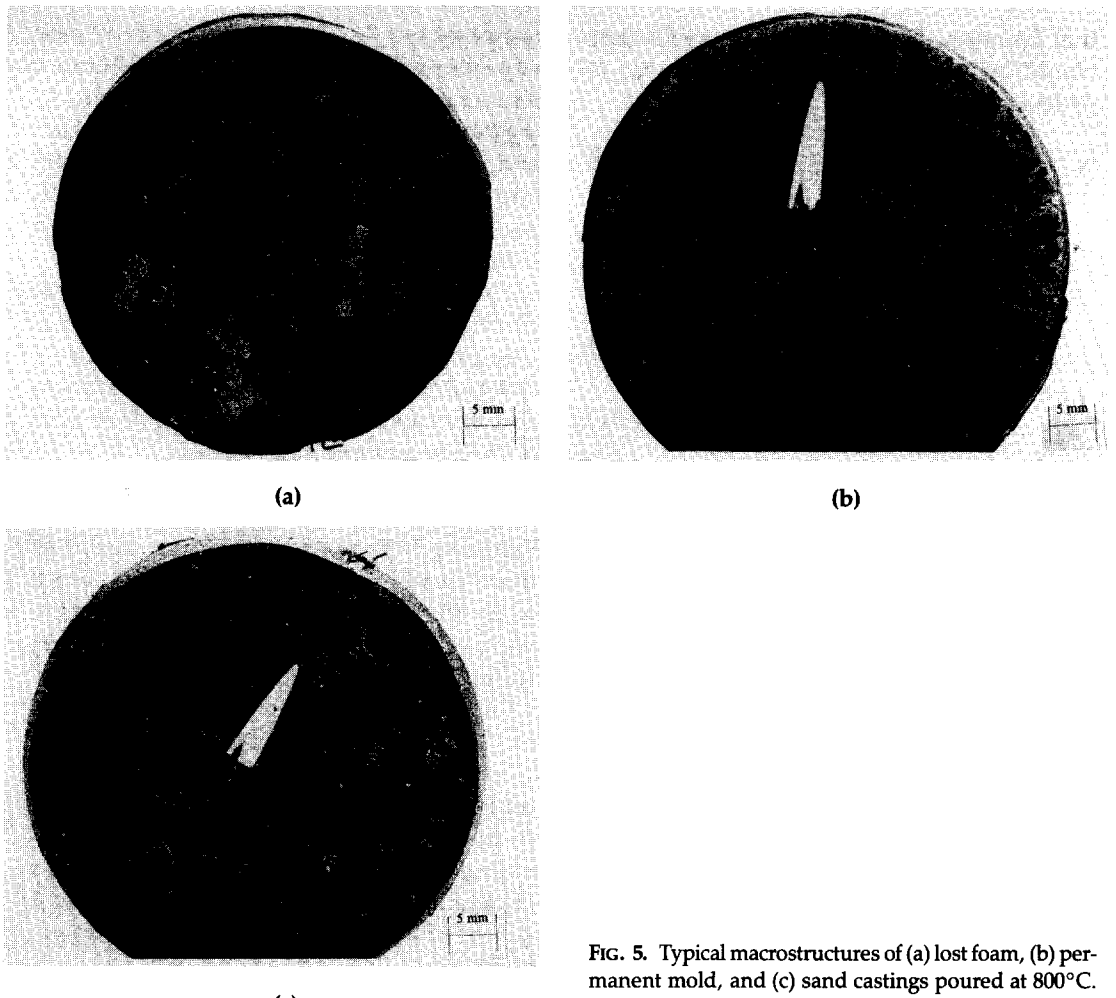

FIG. 5. Typical macrostructures of (a) lost foam, (b) permanent mold, and (c) sand castings poured at 800°C. Etchant: Tucker's reagent.

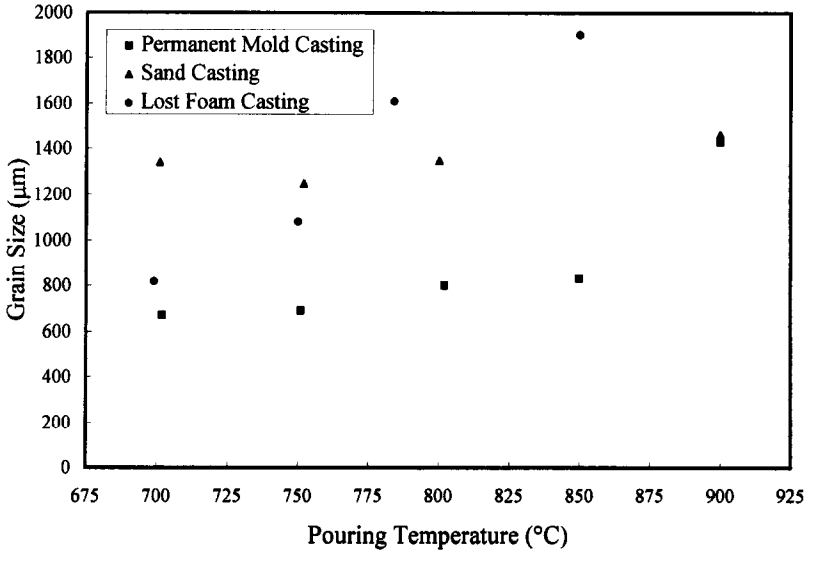

FIG. 6. Variation of grain size with pouring temperatures.

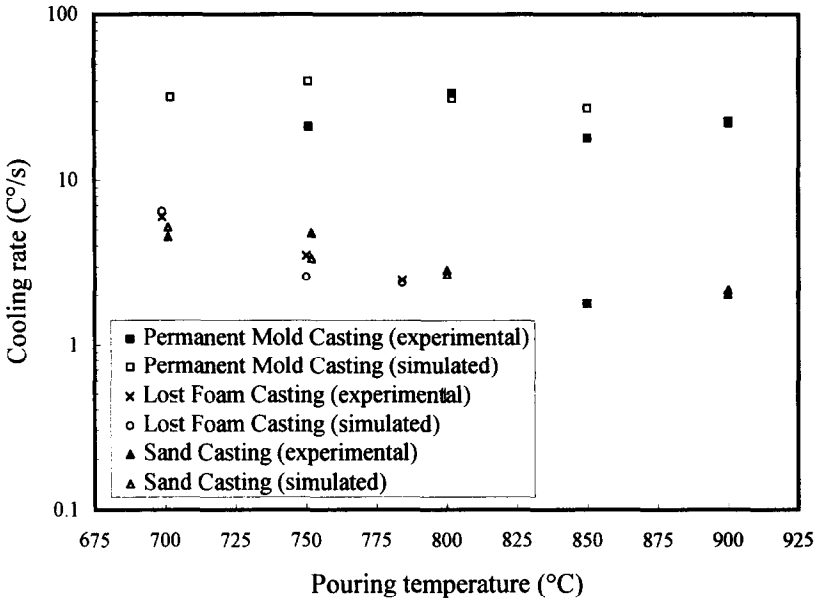

FIG. 7. Variations of cooling rates with pouring temperatures.

650 and 625°C). The variation of experimental cooling rate with pouring temperatures is shown in Fig. 7. The cooling rates decrease with increasing pouring temperatures in sand and lost foam castings. These observations can be attributed to the differences in the heat diffusivity and the heat capacity of the mold materials [21] (Table 2). It can be clearly seen from Table 2 that the ratio of the heat diffusivities of mild steel and green sand is above 400 while that of dry silica sand and green sand is around 6. Also, the presence of the refractory coating between the hot liquid metal and the surrounding dry silica sand mold in lost foam casting leads to a decreased cooling rate relative to sand casting. The maximum temperature recorded by the thermocouple for a pouring temperature of 700°C was less than 650°C for permanent mold casting. Hence, the cooling rate could not be calculated for the pouring temperature of 700°C in permanent mold casting.

The castings were simulated using a macro–micro model. The details of the simulation along with relevant results are provided elsewhere [22]. The simulated cooling rates were calculated in similar temperature ranges and are also shown in Fig. 7. There is a close agreement between the simulated and the experimental cooling rates for all three processes. The values for pouring temperatures of 800 and 900°C match with the experimental values in permanent mold casting. The mismatch for the pouring temperatures of 750 and 850°C can indeed be considered minimal for the experimental conditions. Simulated cooling rates decrease with increasing pouring temperatures except for 700°C. The cooling rate increases initially (up to 750°C) and decreases thereafter. This is to be expected, as most of the heat is utilized to raise the temperature of the mold at lower pouring temperatures. At much higher temperatures (e.g., 800–850°C), however, the mold having reached a saturation

Table 2 Heat Diffusivities, Heat Capacities, and Thermal Diffusivities of the Mold Materials at 625°C

Material	*Heat diffusivity* ($W^2\ m^{-4}\ sK^{-2}$)	*Heat capacity* ($Jm^{-3}\ K^{-1}$)
Mild steel [24]	2.194×10^8	7.281×10^6
Green sand [25]	5.004×10^5	2.859×10^5
Dry silica sand [26]	2.877×10^6	2.915×10^6

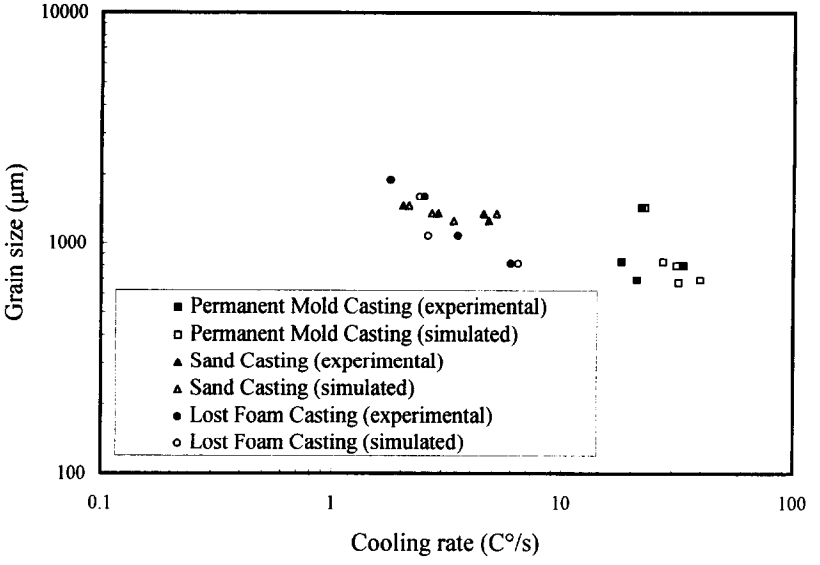

FIG. 8. Variation of grain size with cooling rates.

level does not transfer heat at an increased rate with temperature.

The variation of grain size with the cooling rate is shown in Fig. 8. The grain size can be observed to decrease with increasing cooling rates in all three processes. Few data exist in the literature on the effect of cooling rate on grain size in aluminum-foundry alloys [9]. Fang and Granger [23] have related the grain size with cooling rates. The reported cooling rate [23] has been calculated from the liquidus to the solidus. When the cooling rates were calculated in the same range in the present work, the variation of grain size with the cooling rate is as shown in Fig. 9. There is reasonable agreement in the cooling rate–grain size relationships obtained by Fang and Granger [23] and the present authors. However, the grain size values for permanent mold casting are higher than those obtained by Fang and Granger for similar cooling rates. Shivkumar

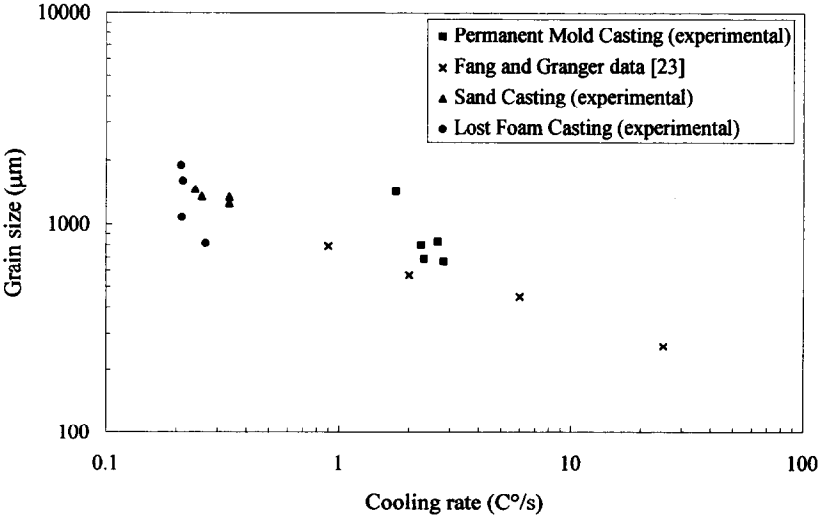

FIG. 9. Variation of grain size with cooling rate (liquidus–solidus; experimental).

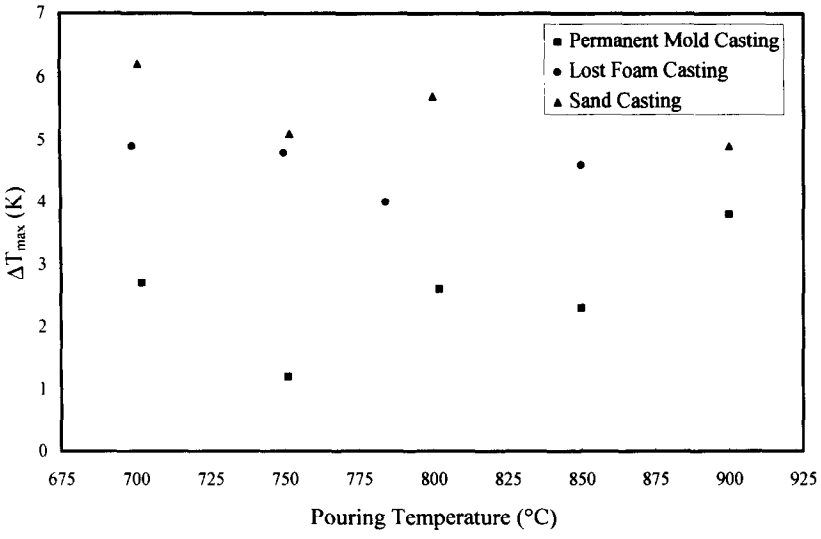

FIG. 10. Variation of ΔT_{max} with pouring temperatures.

et al. [15] have also compared their results (simulated) with those published by Fang and Granger and have obtained reasonable agreement. It is indeed appropriate to expect some variation, for the grain size is strongly dependent on the n_0 value.

ΔT_{max} VALUES

The variations of ΔT_{max} values with pouring temperature are shown in Fig. 10. There is no trend for the variation of ΔT_{max} with pouring temperature in either sand or permanent mold castings. In lost foam castings, however, ΔT_{max} is almost constant with pouring temperature. As mentioned previously, the variation of ΔT_{max} with pouring temperatures is affected by the loss of nucleation sites and by the change in the cooling rates. While a decrease in the number of sites available for nucleation (n_0) would lead to an increase in ΔT_{max}, a decrease in cooling rate would lead to a decrease in ΔT_{max}. Therefore, it is reasonable to suggest that the two factors influence the nucleation process in an opposing manner.

n_0 VALUES

The variations of n_0 values with pouring temperatures are shown for the three processes in Fig. 11. The n_0 values did not significantly vary with pouring temperatures in sand casting. However, they decrease in lost foam casting. A similar trend is not seen in permanent mold casting. Beyond a pouring temperature of around 765°C, the n_0 of lost foam casting becomes less than that of sand casting. This is in accordance with the explanation given earlier for the variation of grain size with pouring temperatures in lost foam castings. The n_0 values for permanent mold casting do not show any trend possibly because of the stronger dependence of cooling rates on pouring temperatures.

As mentioned previously, the n_0 values thus calculated represent the combined effects of the decrease in the number of nucleating sites and the decrease in the cooling rates, with increase in pouring temperatures. This could explain the dependence of n_0 values on the casting process though, ideally, it should be a function of only the melt history. However, a provision to include the pouring temperature for predicting the microstructure would widen the scope of application of the macro–micro model. The n_0 value thus evaluated indicates not only the change in the number of nucleation sites due to the melt superheat, but also the difference in cooling rates in the solidifying casting.

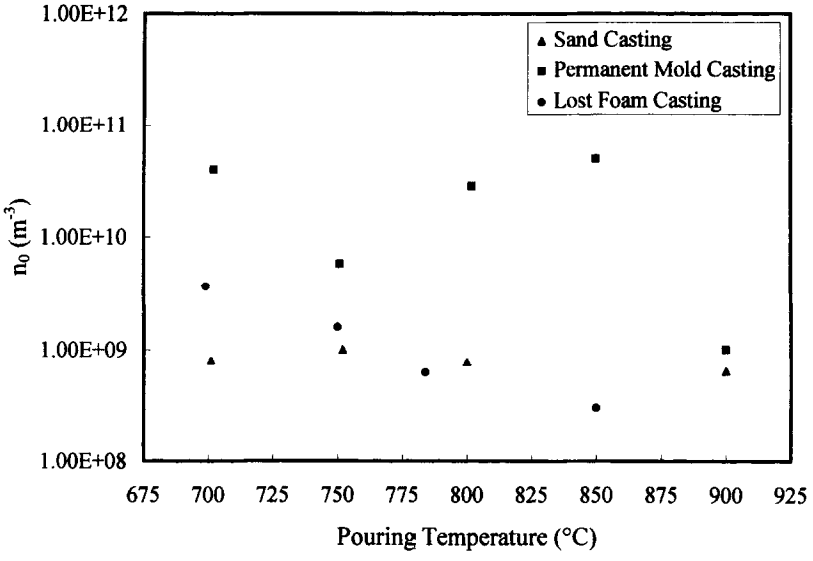

FIG. 11. Variation of n_0 with pouring temperatures.

CONCLUSIONS

Grain size increased with melt superheat in all the three processes. However, the extent of variation in the grain size differed from one casting process to another. When metal was poured at 700°C, the lost foam cast grains were finer than the corresponding sand cast grains. They coarsened progressively with pouring temperatures. Beyond 765°C, they were coarser than the corresponding sand cast grains. This could be due to the foam degradation in lost foam casting leading to a temperature drop at the metal front. This drop could become significant at lower-melt superheats. Cooling rates measured from the experimental data in the temperature range 650–625°C were affected by the pouring temperatures to varying extents in the three casting processes. Cooling rates decreased with increasing pouring temperatures in sand and lost foam castings. A definite trend could not be established in permanent mold castings.

The castings were simulated by using a macro–micro model. The simulated cooling rates were found to decrease with increase in pouring temperatures in sand and lost foam castings. In permanent mold castings, however, this decrease was observed only above a pouring temperature of 750°C. In all three processes, there was fairly close agreement between experimental and simulated cooling rates. Indeed, the agreement was excellent in lost foam and sand castings. Cooling rates were also calculated between the liquidus and solidus temperatures. The grain size–cooling rate relationship agrees well with that available in the literature.

The n_0 values decreased with increasing pouring temperatures in the case of lost foam process while they were practically constant for sand casting in the experimental range of temperatures. A similar trend was not established for permanent mold castings. The n_0 value in this work represents the combination of the decrease in the number of nucleation sites due to dissolution at higher-melt superheats and the decrease in cooling rates due to higher pouring temperatures. It is not possible to experimentally separate one from the other. Beyond a pouring temperature of around 765°C, the n_0 of lost foam casting becomes less than that of sand casting. This is indicative of the chilling effect of the foam on the metal. Such an effect is found to be pronounced at lower pouring temperatures. At higher pouring tempera-

tures, however, the relatively low thermal conductivity of the refractory coating results in a coarser grain size.

The authors are grateful to Dr. W. E. White, Dean of Engineering and Applied Science, Ryerson Polytechnic University for reviewing the manuscript. This research work was supported by a research grant from the Natural Sciences and Engineering Research Council of Canada.

R. Venkataramani is a postdoctoral fellow; R. Simpson is a graduate student, and C. Ravindran is a professor with Ryerson Polytechnic University.

References

1. M. Rappaz, Modelling of microstructure formation in solidification processes, *Int. Mater. Rev.* 34:93–123 (1989).
2. D. M. Stefanescu and C. S. Kanetkar, Modeling of microstructural evolution of eutectic cast iron and of the gray/white transition, *Trans. AFS* 95: 139–144 (1987).
3. Ch.-A. Gandin, M. Rappaz, and R. Tintillier, Three-dimensional probabilistic simulation of solidification grain structures: application to superalloy precision castings, *Metall. Trans. A* 24:467–479 (1993).
4. M. Rappaz and Ch.-A. Gandin, Probabilistic modelling of microstructure formation in solidification processes, *Acta Metall. Mater.* 41:345–360 (1993).
5. G. F. Bolling, *Manipulation of Structure and Properties*, Proc. Sem. on Solidification, American Society for Metals, Metals Park, OH (October 11–12, 1969).
6. R. Venkataramani, N. Gowrishankar, and O. Prabhakar, Microstructure simulation incorporating the effect of melt superheat, *Metals Mater. Processes* 4:151–170 (1992).
7. R. W. Monroe, *Expendable Pattern Casting*, American Foundrymen's Society, Des Plaines, IL (1992).
8. M. C. Flemings, *Solidification Processing*, McGraw-Hill, New York, pp. 193–210 (1974).
9. J. E. Gruzleski and B. M. Closset, Grain refinement, in *The Treatment of Liquid Aluminum-Silicon Alloys*, American Foundrymen's Society, Des Plaines, IL, pp. 127–142 (1990).
10. W. Oldfield, A quantitative approach to casting solidification: freezing of cast iron, *Trans. ASM* 59: 945–959 (1966).
11. D. D. Goettsch and J. A. Dantzig, *Modeling Microstructure Development in Gray Iron Castings*, Proc. Int. Conf. on Modeling of Casting, Welding and Advanced Solidification Processes V, M. Rappaz, M. R. Ozgu, and K. W. Mahin, eds., Minerals, Metals and Materials Society, Warrendale, PA, pp. 377–385 (1990).
12. Ph. Thévoz, Modelisation de la solidification dendritique equiaxe, Ph.D. Thesis, Ecole Polytechnique Federale, Lausanne, Switzerland (1988).
13. H. Biloni and B. Chalmers, Origin of the equiaxed zone in small ingots, *J. Mater. Sci.* 3:139–149 (1968).
14. H. D. Merchant, *Recent Research on Cast Iron*, Proceedings of a Seminar Held in Detroit, Michigan, June 16–18, 1964, Sponsored by the American Society for Metals, Metals Park, Ohio, H. D. Merchant, ed., Gordon and Breach, New York, pp. 15–33 (1968).
15. S. Shivkumar, D. Apelian, and J. Zou, Modeling of microstructure evolution and microporosity formation in cast aluminum alloys, *Trans. AFS* 98: 897–904 (1990).
16. R. Venkataramani, Experimental and theoretical investigations of the equiaxed dendritic and eutectic solidification in Al-7%Si alloy, Ph.D. Thesis, Indian Institute of Technology, Madras, India (1994).
17. *Metals Handbook, Vol. 7: Atlas of Microstructures of Industrial Alloys*, 8th ed., American Society of Metals, Metals Park, OH, pp. 258, 342 (1973).
18. C. H. Su and H. L. Tsai, A direct method to include latent heat effect for modeling casting solidification, *Trans. AFS* 99:781–789 (1991).
19. D. M. Stefanescu, *The Second Generation of Computer Models for Solidification: Heat Transfer–Solidification Kinetics (HT-SK) Codes*, Proc. of the 18th Annual Automotive Materials Symp., Michigan State University, East Lansing, MI (May 1–2, 1991).
20. S. Shivkumar, Casting characteristics of Al alloys in the EPC process, *Trans. AFS* 101:513–518 (1993).
21. J. Campbell, *Castings*, Butterworth-Heinemann, Oxford, pp. 130–131 (1993).
22. R. Venkataramani, R. Simpson, and C. Ravindran, Microstructural modeling of solidification in A356 alloy, *Mater. Char. (in process*, 1995).
23. Q. T. Fang and D. A. Granger, Porosity formation in modified and unmodified A356 alloy castings, *Trans. AFS* 97:989–1000 (1989).
24. *Metals Handbook, Vol. 1: American Society for Metals, Properties and Selections: Irons and Steels, Physical Properties of Carbon and Low-Alloy Steels*, American Society of Metals, Metals Park, OH, pp. 145, 148, 149 (1988).
25. T. S. Prasannakumar, S. D. Pathak, and O. Prabhakar, Finite element formulations for estimating feeding efficiency factors, *Trans. AFS* 93:789–800 (1985).
26. K. Kubo and R. D. Pehlke, Thermal properties of molding sands, *Trans. AFS* 93:405–414 (1985).

Received January 1995; accepted March 1995.

Appendix: Nomenclature

Symbol	*Definition*	*Units*
ΔT	Undercooling	K
$\Delta T'$	Instantaneous undercooling	K
ΔT_N	Undercooling corresponding to the peak of the Gaussian curve	K
ΔT_σ	Range of the Gaussian curve	K
ΔT_{max}	Maximum undercooling experienced	K
A	Constant	$m^{-3}\ K^{-2}$
erf(..)	Error function	–
K_1, K_2	Constants	s^{-1}, K^3
N	Number of sites available for nucleation	m^{-3}
$\dot{n}$	Nucleation rate	$m^{-3}\ s^{-1}$
n	Nuclei density	m^{-3}
n_a	Actual number of nuclei present per unit volume	m^{-3}
n_0	Maximum nuclei density	m^{-3}
R_a	Actual radius measured	m
T	Temperature	K
T_1	Temperature of the onset of recoalescence	K
T_i	Initial temperature	K
T_L	Liquidus temperature	K
T_∞	Ambient temperature	K
t	Time	s
Y	Nondimensional temperature: $\frac{T - T_\infty}{T_i - T_\infty}$	–
β	A constant = $\sqrt{2\pi}\left(\frac{\Delta T_\sigma}{n_0}\right)$	m^3 K
ξ	Nondimensional undercooling: $\frac{\Delta T' - \Delta T_N}{\sqrt{2}\Delta T_\sigma}$	–